Electronic Supplementary Material (ESI) for ChemComm.

Chelate-Free “Turn-ON” -Type Fluorescence Detection of Trivalent Metal Ions

Shota Matsumoto,[a] Tomohiro Umeno,[a] Noriko Suzuki,[a] Kazuteru Usui,[a] Masatoshi Kawahata,[a] and Satoru Karasawa*[a]

[a] Faculty of Pharmaceutical Sciences, Showa Pharmaceutical University, 3-3165 Higashi-tamagawagakuen, Machida 194-8543, Japan. karasawa@ac.shoyaku.ac.jp (S.K.)

Table of Contents

General Information

^{1}H, ^{13}C and ^{19}F-NMR

The proton (^{1}H), carbon-13 (^{13}C), and fluorine-19 (^{19}F) nuclear magnetic resonance (NMR) spectra were measured on a Bruker Biospin AVANCE II 600 or III 300 spectrometer employing $CDCl_3$, CD_3OD, or Acetone-d_6 as the solvent. Chemical shifts (δ) are reported in parts per million (ppm). For ^{1}H NMR spectra ($CDCl_3$), tetramethylsilane was used as the internal reference (0.00 ppm), while the central solvent peak as the reference (77.0 ppm in $CDCl_3$, 49.0 ppm in CD_3OD and 29.9 ppm in Acetone-d_6) for ^{13}C NMR spectra.

IR spectra

The infrared (IR) spectra for the samples were recorded by the tablet method using KBr or the thin-film method using NaCl plates on a JASCO FT/IR-420 spectrometer.

HRMS

The high-resolution electrospray ionization mass spectra were recorded on a JEOL JMS-T 100LP spectrometer.

UV−vis and Fluorescence Spectroscopy and Fluorescence Quantum Yield Measurements

The ultraviolet−visible (UV−vis) spectra of the solutions were recorded on JASCO V-760 spectrometers. The fluorescence spectra and fluorescence quantum yield of solutions were determined on a JASCO FP-8500 spectrofluorimeter that was equipped with a calibrated integrating sphere system.

X-ray Crystallography

The single-crystal X-ray diffraction data were collected on a Rigaku XtaLAB Synergy Custom and RA-Micro7 HFM diffractometers, which were equipped with graphite-monochromated Cu Kα radiation (λ = 1.54187 Å) and HyPix-6000HE detector at 93 ± 1 K. The structure was solved with the ShelXT[1] structure solution program using the Intrinsic Phasing solution method and by using Olex2[2] as the graphical interface. The model was refined with ShelXL[3] using Least Squares minimisation. The non-hydrogen atoms were refined anisotropically, whereas the hydrogen atoms were refined isotropically or, for those bonded to C atoms, using a riding model. Crystallographic data files (CIF) for the structures reported in this paper have been deposited with the Cambridge Crystallographic Data Center (CCDC) as supplementary publication nos. CCDC-2194442 for **INA-DEA** and CCDC-2194212 for $[Al^{III}(H_2O)_6$ [**INA-DMA-H**$]^{+}{}_2]Cl_5$.

p*K*a Determination

The p*K*a values were determined via UV−vis spectroscopy, as described in our previous work.[4] The 20 μM solutions **INA** analogs containing 30% (v/v) 1,4-dioxane/buffer were used as the working solutions. Buffer solutions with different pH values were prepared using the Britton−Robinson buffer (pH 2-13) and the HCl-KCl (pH 1-2) buffer. The pH of the buffer solutions was monitored by a HORIBA D-51 pH meter equipped with a glass electrode (HORIBA 9681S-10D).
The p*K*a values of **INA** analogs were worked out by nonlinear regression (Igor Pro 9) using eq 1 as reported.[5]

$$Absorbance\ total = \frac{\varepsilon_{\mathrm{HA}} - \varepsilon_{\mathrm{A}^-} \times \left[10^{(\mathrm{pH}-\mathrm{p}Ka)}\right]}{1 + 10^{(\mathrm{pH}-\mathrm{p}Ka)}} \times [\mathrm{S_t}] \qquad (1)$$

where ε_{HA} and ε_{A-} are the extinction coefficients of the acid and base forms of the compound, respectively, and $[S_t]$ is the total compound concentration.

Materials

Analytical thin layer chromatography (TLC) was performed with Merck Millipore pre-coated TLC plates, silica gel 60 F254, layer thickness 0.25 mm. Compounds were observed in UV-light at 254 nm. Flash chromatography separations were performed on Kanto Chemical silica gel 60N, spherical neutral, particle size 40-50 μm. Reagents and solvents were commercial grade and were used as supplied, unless otherwise noted.

Experimental

Scheme S1. Synthetic routes of **INA** analogs.

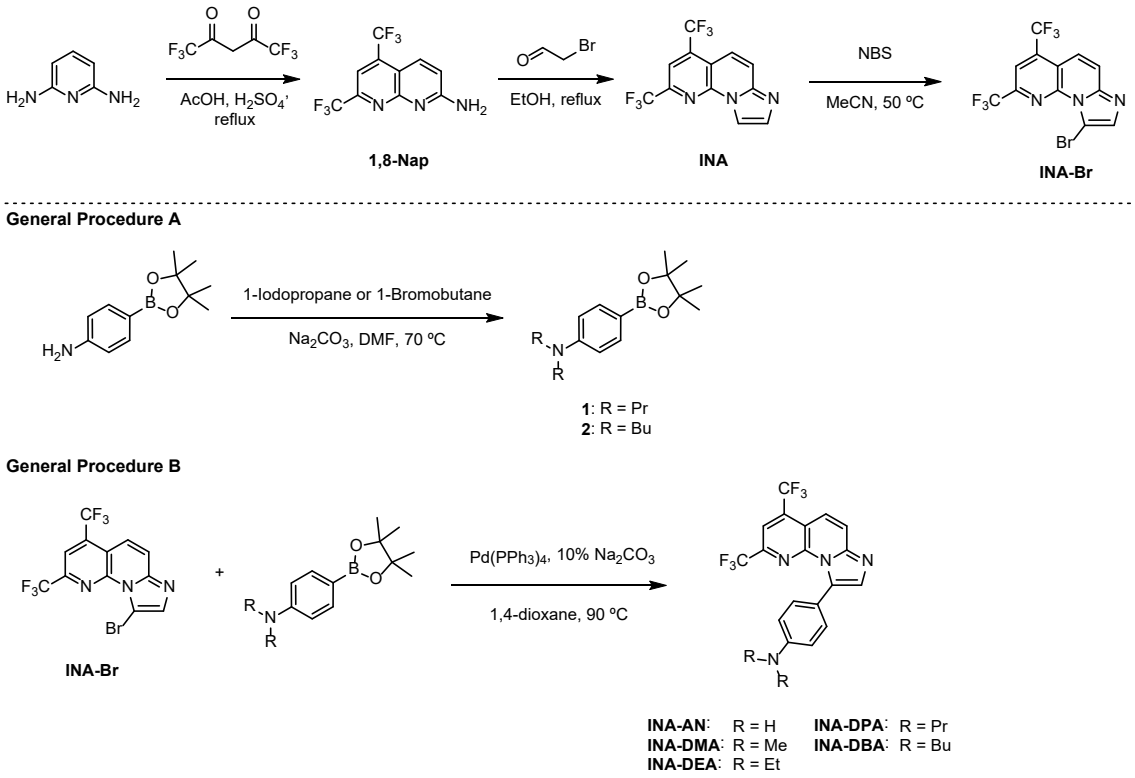

We synthesized 5,7-bis(trifluoromethyl)-1,8-naphthyridin-2-amine (**18–Nap**), 2,4-bis(trifluoromethyl)imidazo[1,2-*a*][1,8]naphthyridine (**INA**), 9-bromo-2,4-bis(trifluoromethyl)imidazo[1,2-*a*][1,8]naphthyridine (**INA–Br**), 9-phenyl-2,4-bis(trifluoromethyl)imidazo[1,2-*a*][1,8]naphthyridine (**INA-Ph**) and 4-(2,4-bis(trifluoromethyl)imidazo[1,2-*a*][1,8]naphthyridin-9-yl)-N,N-dimethylaniline (**INA-DMA**) using previously reported methods.[4,6-7]

General Procedure A (Synthesis of **1**−**2**):
To a DMF (0.37 M) solution containing 4-(4,4,5,5-tetramethyl-1,3,2-dioxaborolan-2-yl)aniline (1.0 equiv) and Na_2CO_3 (2.0 equiv), 1-Iodopropane (4.0 equiv) or 1-Bromobutane (4.0 equiv) was added and heated 70 ºC for 1.5−3 h. The resulting mixture was extracted three times with *n*-Hexane/AcOEt (4:1, v/v), and the combined organic layer was dried successively over Na_2SO_4 and in a vacuum. Further, the residue was purified by flash column chromatography on silica gel to give **1**−**2**.

General Procedure B (Synthesis of **INA-DEA**, **INA-DPA** and **INA-DPA**):
A 10% Na_2CO_3 aqueous solution was added to a 1,4-dioxane solution (0.1 M) of **INA-Br** (1.0 equiv), dioxaborolane (1.1 or 1.2 equiv), and tetrakis(triphenylphosphine) palladium (0) (5 or 10 mol%) in an N_2 atmosphere and stirred for 1-16 h at 90 °C. The resulting mixture was extracted three times with CH_2Cl_2, and the combined organic layer was dried successively over Na_2SO_4 and in a vacuum. Further, the residue was purified by flash column chromatography on silica gel to give **INA** derivatives.

Synthesis of *N,N*-dipropyl-4-(4,4,5,5-tetramethyl-1,3,2-dioxaborolan-2-yl)aniline (**1**):
By following general procedure A, the reaction of 4-(4,4,5,5-tetramethyl-1,3,2-dioxaborolan-2-yl)aniline (1.0 g, 4.6 mmol) yielded the desired product **1** (857 mg, 61%) as a white solid.
R_f = 0.41 (*n*-hexane/AcOEt 9:1);m.p. 74–75 ºC; ^{1}H NMR (300 MHz, Acetone-d_6) δ 7.54 (d, J = 8.9 Hz, 2H), 6.64 (d, J = 8.9 Hz, 2H), 3.31 (t, J = 7.7 Hz, 4H), 1.61 (sext, J = 7.5 Hz, 4H), 1.28 (s, 12H), 0.92 (t, J = 7.4 Hz, 6H); ^{13}C NMR (151 MHz, Acetone-d_6) δ 151.3, 137.1, 114.8, 111.4, 83.6, 53.0, 25.2, 21.0, 11.5; IR (KBr): 3087, 2972, 2934, 2876, 1602, 1360, 1143 cm^{-1}; HRMS (ESI): *m*/*z* calcd for $C_{18}H_{30}BNO_2$+H$^+$: 304.2448 [*M*+H]$^+$; found: 304.2441.

Synthesis of *N,N*-dibutyl-4-(4,4,5,5-tetramethyl-1,3,2-dioxaborolan-2-yl)aniline (**2**):
By following general procedure A, the reaction of 4-(4,4,5,5-tetramethyl-1,3,2-dioxaborolan-2-yl)aniline (200 mg, 913 μmol) yielded the desired product **2** (166 mg, 55%) as a colorless oil.
R_f = 0.37 (*n*-hexane/diethyl ether 9:1); ^{1}H NMR (300 MHz, Acetone-d_6) δ 7.55 (d, J = 8.9 Hz, 2H), 6.64 (d, J = 8.9 Hz, 2H), 3.34 (t, J = 7.6 Hz, 4H), 1.63–1.49 (m, 4H), 1.43–1.28 (m, 16H), 0.95 (t, J = 7.3 Hz, 6H); ^{13}C NMR (151 MHz, Acetone-d_6) δ 151.2, 137.1, 114.8, 111.4, 83.6, 51.0, 30.1, 25.2, 20.8, 14.3; IR (NaCl): 3091, 2957, 2931, 2872, 1604, 1361, 1143 cm^{-1}; HRMS (ESI): *m*/*z* calcd for $C_{20}H_{34}BNO_2$+H$^+$: 332.2761 [*M*+H]$^+$; found: 332.2770.

Synthesis of 4-(2,4-bis(trifluoromethyl)imidazo[1,2-*a*][1,8]naphthyridin-9-yl)-*N*,*N*-diethylaniline (**INA-DEA**):

By following general procedure B, the reaction of **INA-Br** (25 mg, 65 μmol) yielded the desired product **INA-DEA** (24 mg, 83%) as a reddish solid.
R_f=0.37 (*n*-hexane/AcOEt 3:1); m.p. 107–109 ºC; ^{1}H NMR (300 MHz, CD_3OD) δ 8.14 (s, 1H), 7.86 (s, 2H), 7.52 (s, 1H), 7.35 (d, *J* = 8.9 Hz, 2H), 6.72 (d, *J* = 9.0 Hz, 2H), 3.44 (q, *J* = 7.0 Hz, 4H), 1.20 (t, *J* = 7.0 Hz, 6H); ^{13}C NMR (151 MHz, CD_3OD) δ 149.2, 146.8, 145.9, 145.5 (q, *J* = 34.1 Hz), 137.9 (q, *J* = 34.1 Hz), 134.3, 133.7, 132.4, 124.0 (q, *J* = 274.7 Hz), 123.4, 121.9 (q, *J* = 274.4 Hz), 120.3, 119.5, 118.2, 115.0, 112.2, 45.6, 12.8; ^{19}F NMR (282 MHz, $CDCl_3$) δ -60.90 (d, *J* = 1.8 Hz), -67.11; IR (KBr): 3042, 2974, 2935, 1612, 1492, 1402, 1282, 1136 cm^{-1}; HRMS (ESI): *m*/*z* calcd for $C_{22}H_{18}F_6N_4$+H$^+$: 453.1514 [*M*+H]$^+$; found, 453.1551.

Synthesis of 4-(2,4-bis(trifluoromethyl)imidazo[1,2-*a*][1,8]naphthyridin-9-yl)-*N,N*-dipropylaniline (**INA-DPA**):
By following general procedure B, the reaction of **INA-Br** (20 mg, 52 μmol) yielded the desired product **INA-DPA** (23 mg, 94%) as a reddish solid.
R_f = 0.50 (*n*-hexane/AcOEt 1:1); m.p. 83–85 ºC; ^{1}H NMR (300 MHz, Acetone-d_6) δ 8.24 (s, 1H), 7.96 (d, *J* = 9.7 Hz, 1H), 7.85 (qd, *J* = 1.9, 9.7 Hz, 1H), 7.61 (s, 1H), 7.50 (d, *J* = 8.6 Hz, 2H), 6.81 (br, 2H), 3.42 (t, *J* = 7.6 Hz, 4H), 1.72 (sext, *J* = 7.4 Hz, 4H), 0.99 (t, *J* = 7.4 Hz, 6H); ^{13}C NMR (151 MHz, Acetone-d_6) δ 149.0, 146.7, 145.5, 144.3 (q, *J* = 36.8 Hz), 136.9 (q, *J* = 32.8 Hz), 134.8, 133.4, 132.1, 124.4, 123.7 (q, *J* = 274.5 Hz), 123.5 (q, *J* = 457.2 Hz), 119.4, 118.8, 118.0, 114.5, 111.5, 53.4, 21.0, 11.5; ^{19}F NMR (282 MHz, Acetone-d_6) δ -61.43 (d, *J* = 1.7 Hz), -67.44; IR (KBr): 3034, 2963, 2935, 2876, 1611, 1492, 1282, 1138 cm^{-1}; HRMS (ESI): *m*/*z* calcd for $C_{24}H_{22}F_6N_4$+H$^+$: 481.1827 [*M*+H]$^+$; found: 481.1846.

Synthesis of 4-(2,4-bis(trifluoromethyl)imidazo[1,2-*a*][1,8]naphthyridin-9-yl)-*N,N*-dibutylaniline (**INA-DBA**):
By following general procedure B, the reaction of **INA-Br** (155 mg, 469 μmol) yielded the desired product **INA-DBA** (122 mg, 61%) as a reddish solid.
R_f=0.70 (*n*-hexane/AcOEt 1:1); m.p. 75–77 ºC; ^{1}H NMR (300 MHz, Acetone-d_6) δ 8.20 (s, 1H), 7.92 (d, *J* = 9.7 Hz, 1H), 7.81 (qd, *J* = 1.9, 9.7 Hz, 1H), 7.59 (s, 1H), 7.46 (d, *J* = 8.9 Hz, 2H), 6.75 (d, *J* = 8.8 Hz, 2H), 3.41 (t, *J* = 7.6 Hz, 4H), 1.66 (quin, *J* = 7.6 Hz, 4H), 1.41 (sext, *J* = 7.4 Hz, 4H), 0.98 (t, *J* = 7.3 Hz, 6H); ^{13}C NMR (151 MHz, Acetone-d_6) δ 148.0, 145.7, 144.6, 143.3 (q, *J* = 36.8 Hz, 1C), 135.9 (q, *J* = 32.9 Hz, 1C), 133.8, 132.6, 131.0, 123.4, 122.7 (q, *J* = 274.6 Hz), 122.5 (q, *J* = 458.0 Hz), 118.4, 117.7, 116.9, 113.5, 110.6, 50.4, 29.2, 19.9, 13.3; ^{19}F NMR (282 MHz, Acetone-d_6) δ -61.43 (d, *J* = 1.8 Hz), -67.39; IR (KBr): 3046, 2958, 2932, 2874, 1609, 1490, 1282, 1137 cm^{-1}; HRMS (ESI): *m*/*z* calcd for $C_{26}H_{26}F_6N_4$+H$^+$: 509.2140 [*M*+H]$^+$; found: 509.2123.

Photophysical properties in various solvents with different polarities.

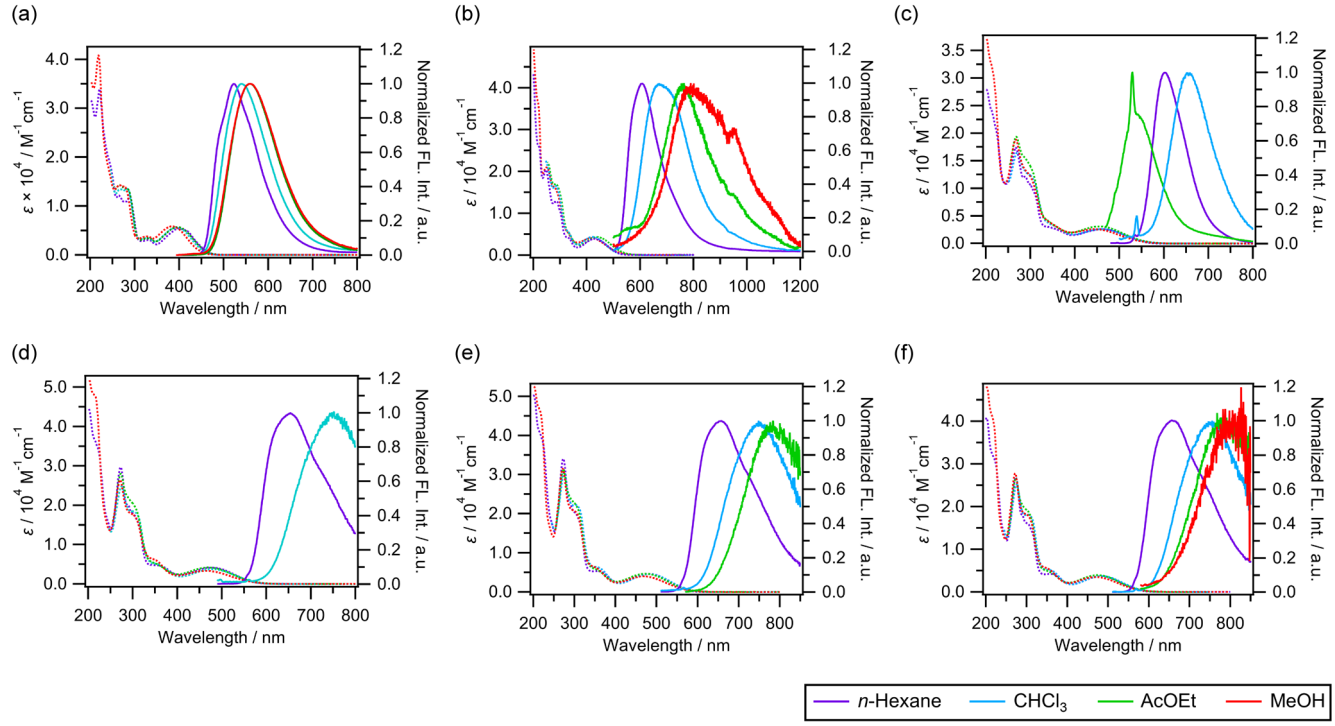

Figure S1. Absorption (dotted lines on the left axis) and fluorescence (solid lines on the right axis) spectra of (a) **INA-Ph**, (b) **-AN**, (c) **-DMA**, (d) **-DEA**, (e) **-DPA**, (f) **-DBA** in various solvents (20 μM). The purple, sky-blue, light green, and red lines indicate conditions using *n*-hexane, $CHCl_3$, AcOEt, and MeOH, respectively.

Table S1. Values of absorption maxima (λ_{max}^{Ab}), fluorescence maxima (λ_{max}^{Fl})[a] and fluorescence quantum yield (Φ^{Fl})[a] of **INA** analogs

	n-Hexane			$CHCl_3$			AcOEt			MeOH		
INAs	λ_{max}^{Ab}	λ_{max}^{Fl}	Φ^{Fl}%	λ_{max}^{Ab}	λ_{max}^{Fl}	Φ^{Fl}%	λ_{max}^{Ab}	λ_{max}^{Fl}	Φ^{Fl}%	λ_{max}^{Ab}	λ_{max}^{Fl}	Φ^{Fl}%
-Ph	399	523	76.6	393	540	61.5	398	559	41.2	383	560	27.3
-AN	427	608	11.5	423	672	1.7	440	765	<0.1	420	790	<0.1
-DMA	462	603	4.4	463	653	0.5	457	537	14.0	444	n.d.[b]	n.d.[b]
-DEA	479	654	4.9	479	753	0.5	471	n.d.[b]	n.d.[b]	465	n.d.[b]	n.d.[b]
-DPA	483	659	5.4	483	749	0.7	472	784	0.5	468	n.d.[b]	n.d.[b]
-DBA	485	658	0.7	485	756	<0.1	476	769	<0.1	468	804	<0.1

[a] Excited at absorption maxima. [b] n.d.: not determined.

pH-dependent absorption and fluorescence spectral change and determination of p*K*a of INA analogs

Scheme S2. Equilibrium of **INA-Ph**

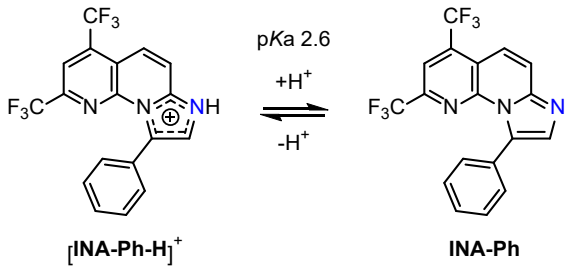

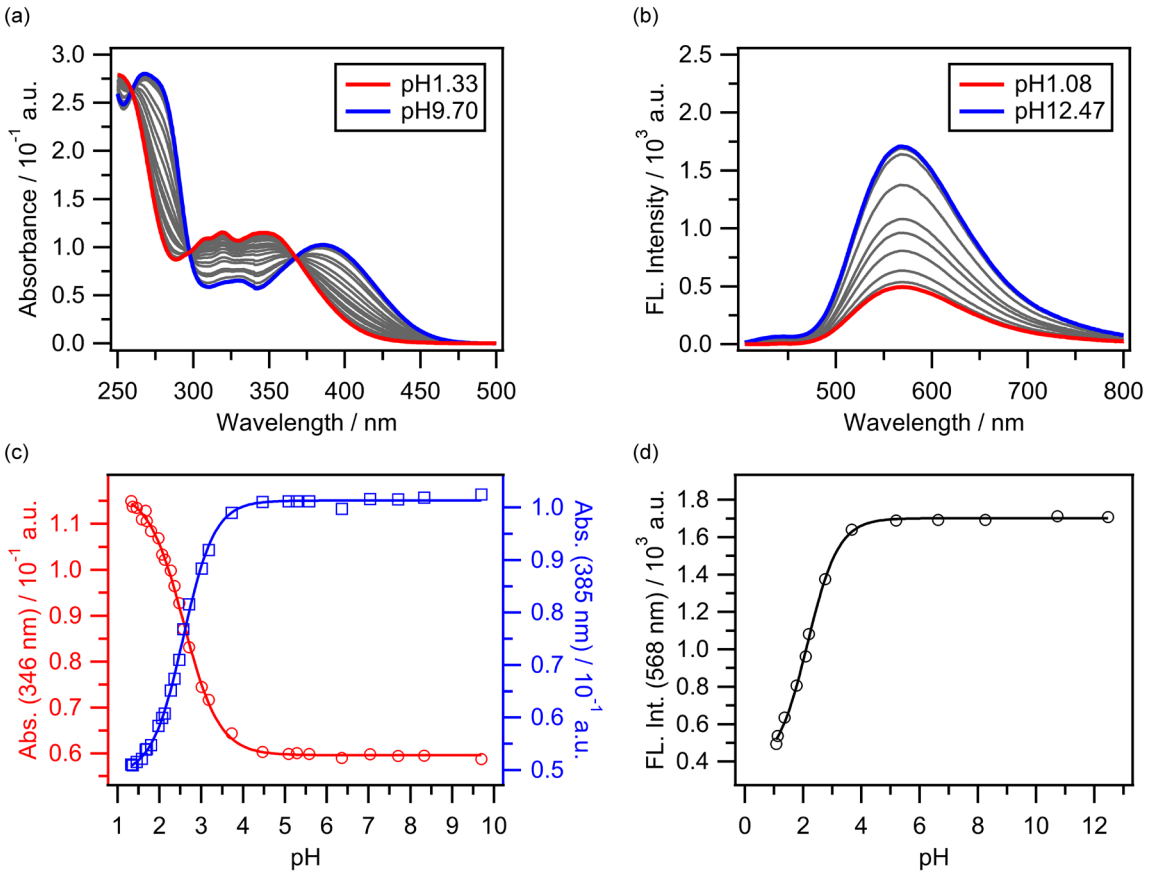

Figure S2. pH titrations of **INA-Ph** in 1,4-dioxane/buffer (3:7, v/v) solutions (20 μM). (a) and (b) represent absorption and fluorescence spectral changes. (c) and (d) are plots of absorption and fluorescence spectral changes as a function of pH values.

Table S2. Values of absorption maxima (λ_{max}^{Ab}), fluorescence maxima (λ_{max}^{Fl})[a] and fluorescence quantum yield (Φ^{Fl})[a] of **INA-Ph**[b] and [**INA-Ph-H**]$^{+}$[c].

	[**INA-Ph-H**]$^{+}$	**INA-Ph**
λ_{max}^{Ab} / nm	346	385
λ_{max}^{Fl} / nm	568	569
Φ^{Fl}%	14.2	7.3

[a] Excited at 385 nm. [b] pH 12.47. [c] pH 1.08.

Scheme S3. Equilibrium of **INA-DMA**

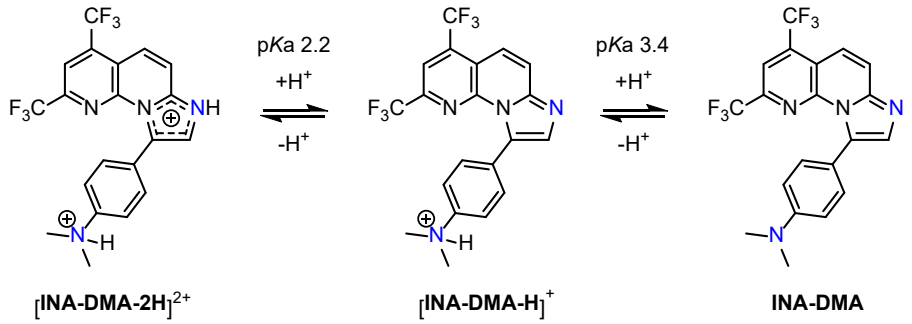

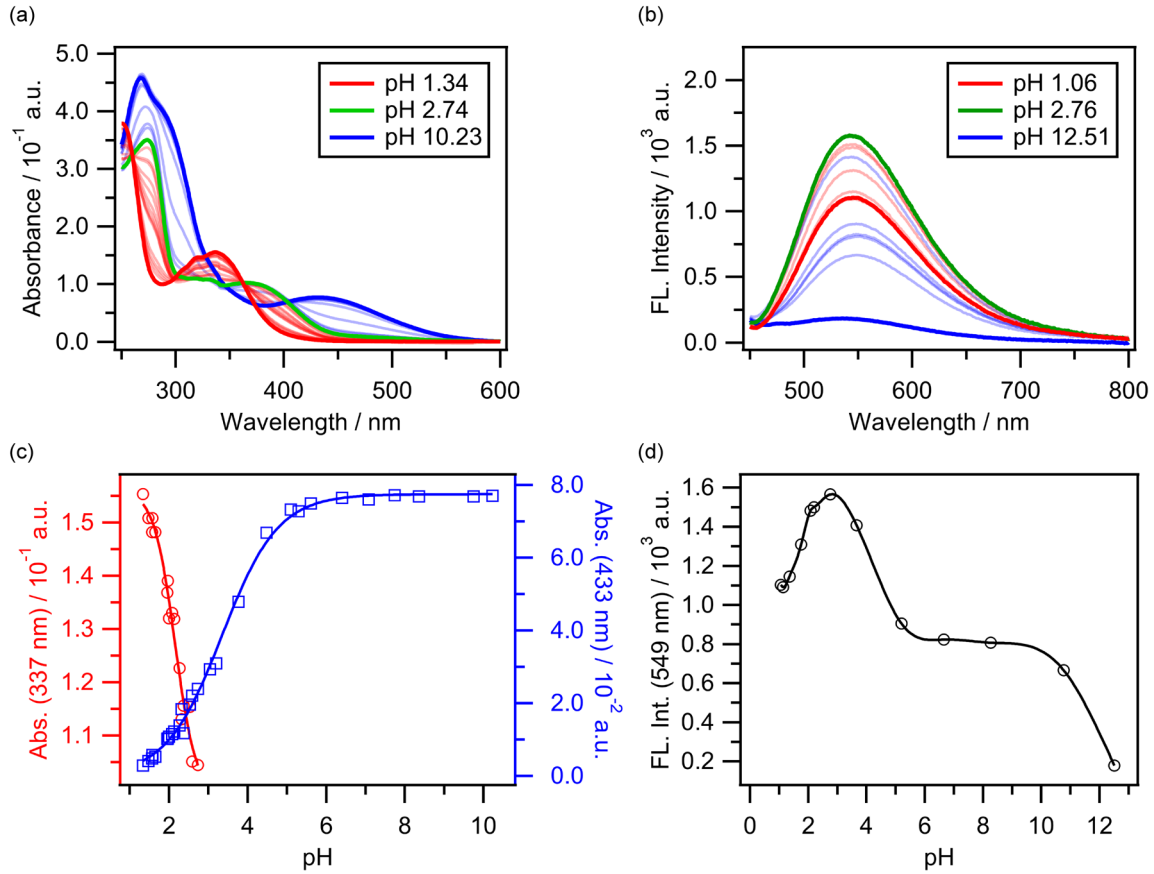

Figure S3. pH titrations of **INA-DMA** in 1,4-dioxane/buffer (3:7, v/v) solutions (20 μM). (a) and (b) represent absorption and fluorescence spectral changes. (c) and (d) are plots of absorption and fluorescence spectral changes as a function of pH values.

Table S3. Values of absorption maxima (λ_{max}^{Ab}), fluorescence maxima (λ_{max}^{Fl})[a] and fluorescence quantum yield (Φ^{Fl})[a] of **INA-DMA**,[b] [**INA-DMA-H**]$^{+}$[c] and [**INA-DMA-2H**]$^{2+}$[d].

	[INA-DMA-2H]$^{2+}$	[INA-DMA-H]$^{+}$	INA-DMA
λ_{max}^{Ab} / nm	337	371	433
λ_{max}^{Fl} / nm	545	549	537
Φ^{Fl}%	1.1	1.1	0.3

[a] Excited at 371 nm. [b] pH 12.51. [c] pH 2.76. [d] pH 1.06.

Scheme S4. Equilibrium of **INA-DPA**

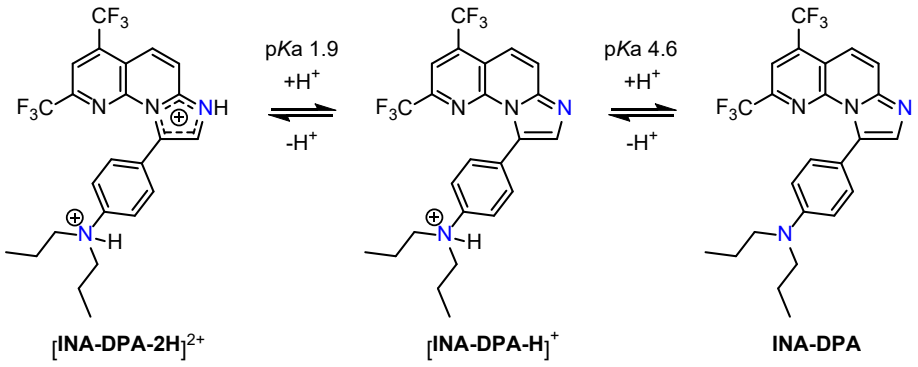

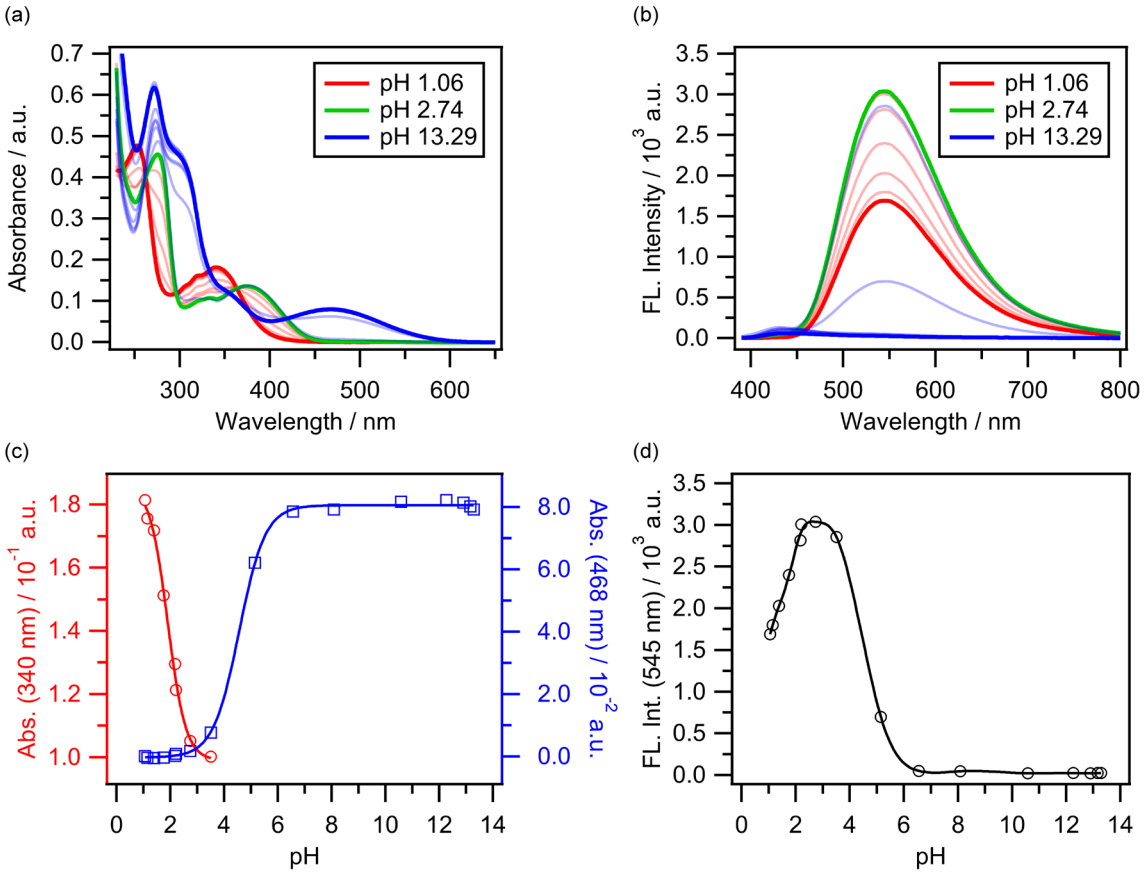

Figure S4. pH titrations of **INA-DPA** in 1,4-dioxane/buffer (3:7, v/v) solutions (20 μM). (a) and (b) represent absorption and fluorescence spectral changes. (c) and (d) are plots of absorption and fluorescence spectral changes as a function of pH values.

Table S4. Values of absorption maxima (λ_{max}^{Ab}), fluorescence maxima (λ_{max}^{Fl})[a] and fluorescence quantum yield (Φ^{Fl})[a] of **INA-DPA**,[b] [**INA-DPA-H**]$^+$ [c] and [**INA-DPA-2H**]$^{2+}$.[d]

	[**INA-DPA-2H**]$^{2+}$	[**INA-DPA-H**]$^+$	**INA-DPA**
λ_{max}^{Ab} / nm	340	374	468
λ_{max}^{Fl} / nm	545	545	432
Φ^{Fl}%	15.4	17.6	1.1

[a] Excited at 374 nm. [b] pH 13.29. [c] pH 2.74. [d] pH 1.06.

Scheme S5. Equilibrium of **INA-DBA**

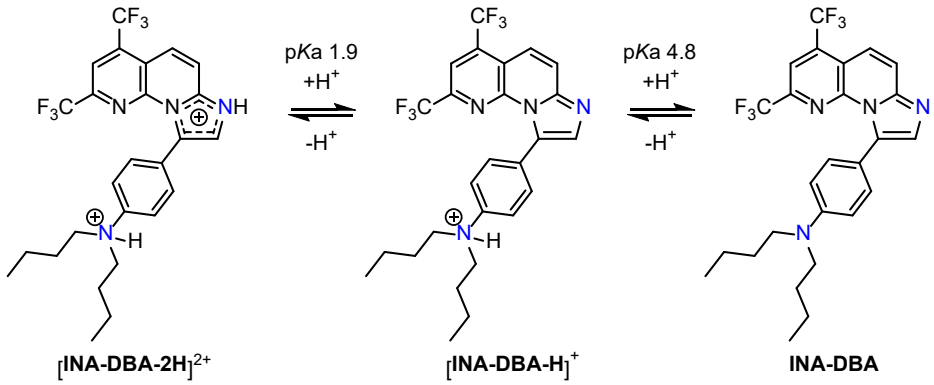

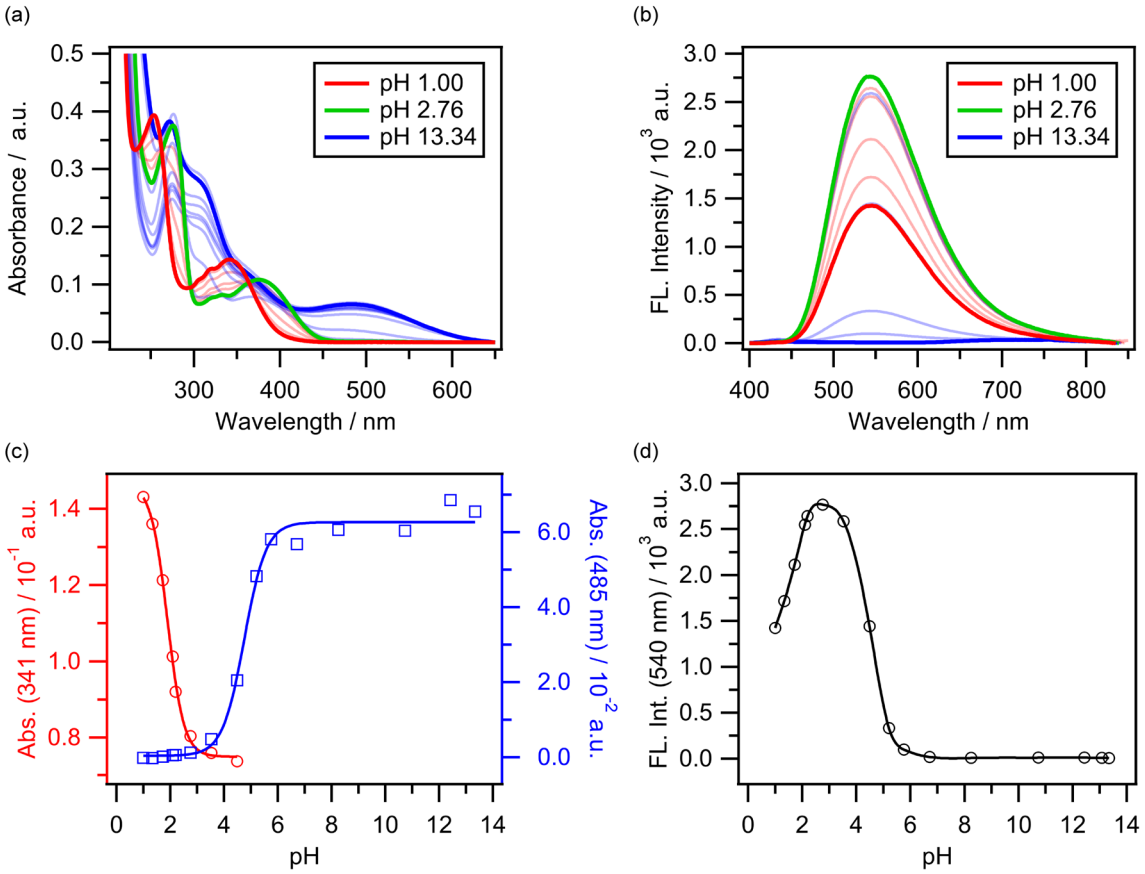

Figure S5. pH titrations of **INA-DBA** in 1,4-dioxane/buffer (3:7, v/v) solutions (20 μM). (a) and (b) represent absorption and fluorescence spectral changes. (c) and (d) are plots of absorption and fluorescence spectral changes as a function of pH values.

Table S5. Values of absorption maxima (λ_{max}^{Ab}), fluorescence maxima (λ_{max}^{Fl})[a] and fluorescence quantum yield (Φ^{Fl})[a] of **INA-DBA**,[b] [**INA-DBA-H**]$^+$ [c] and [**INA-DBA-2H**]$^{2+}$.[d]

	[**INA-DBA-2H**]$^{2+}$	[**INA-DBA-H**]$^+$	**INA-DBA**
λ_{max}^{Ab} / nm	341	377	485
λ_{max}^{Fl} / nm	546	540	436
Φ^{Fl}%	17.8	19.3	0.3

[a] Excited at 377 nm. [b] pH 13.34. [c] pH 2.76. [d] pH 1.00.

The absorption and fluorescence spectral changes upon additions of various metal ions

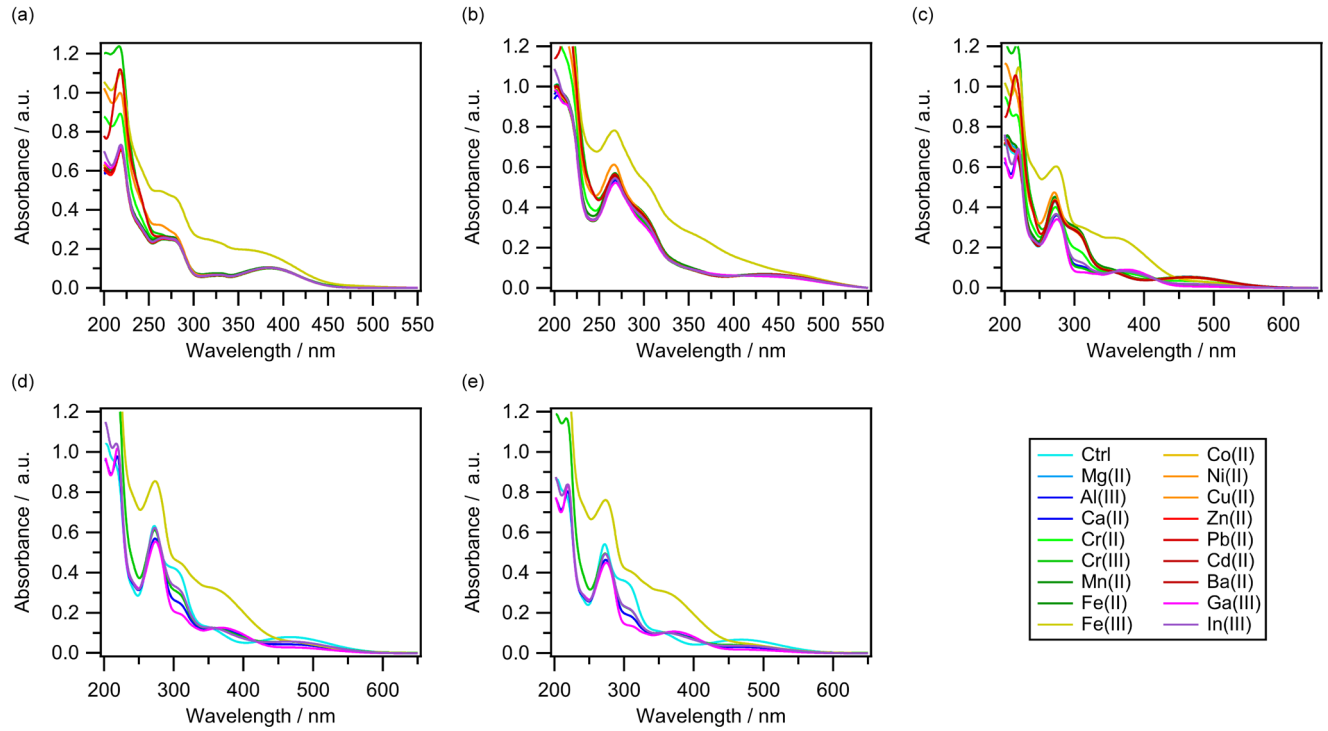

Figure S6. Absorption spectral changes of **INA-Ph** (a), **-DMA** (b), **-DEA** (c), **-DPA** (d), and **-DBA** (e) solutions (20 μM) upon additions of di- and trivalent ions (5 equivalent).

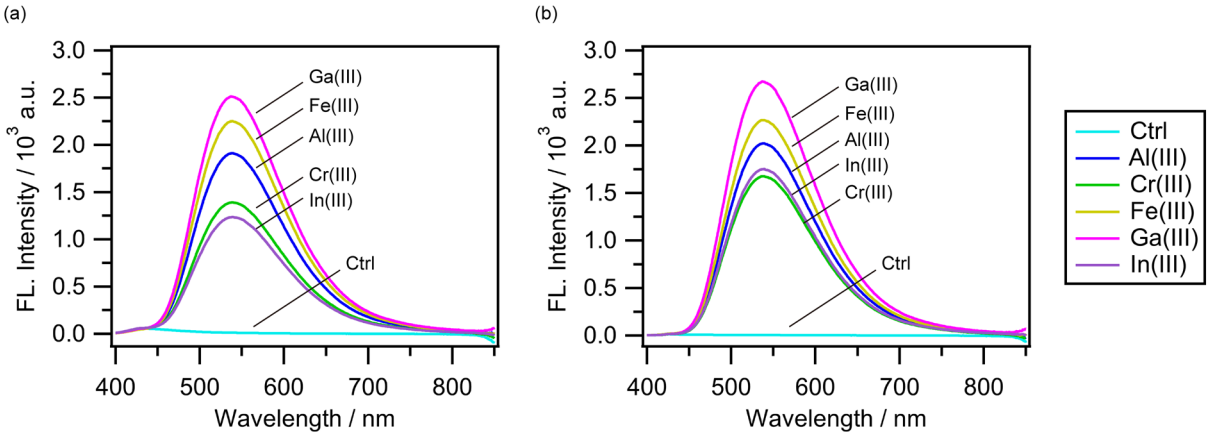

Figure S7. Fluorescence spectral changes of **INA-DPA** (a), and **-DBA** (b) solutions (20 μM) upon additions of di- and trivalent ions (5 equivalent).

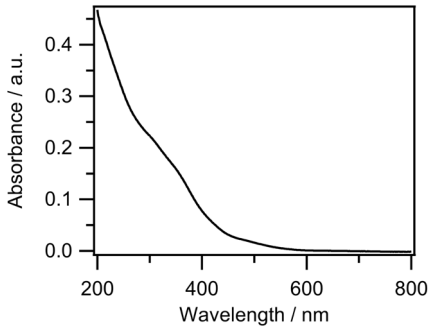

Figure S8. Absorption spectrum of Fe^{III} solution (100 μM).

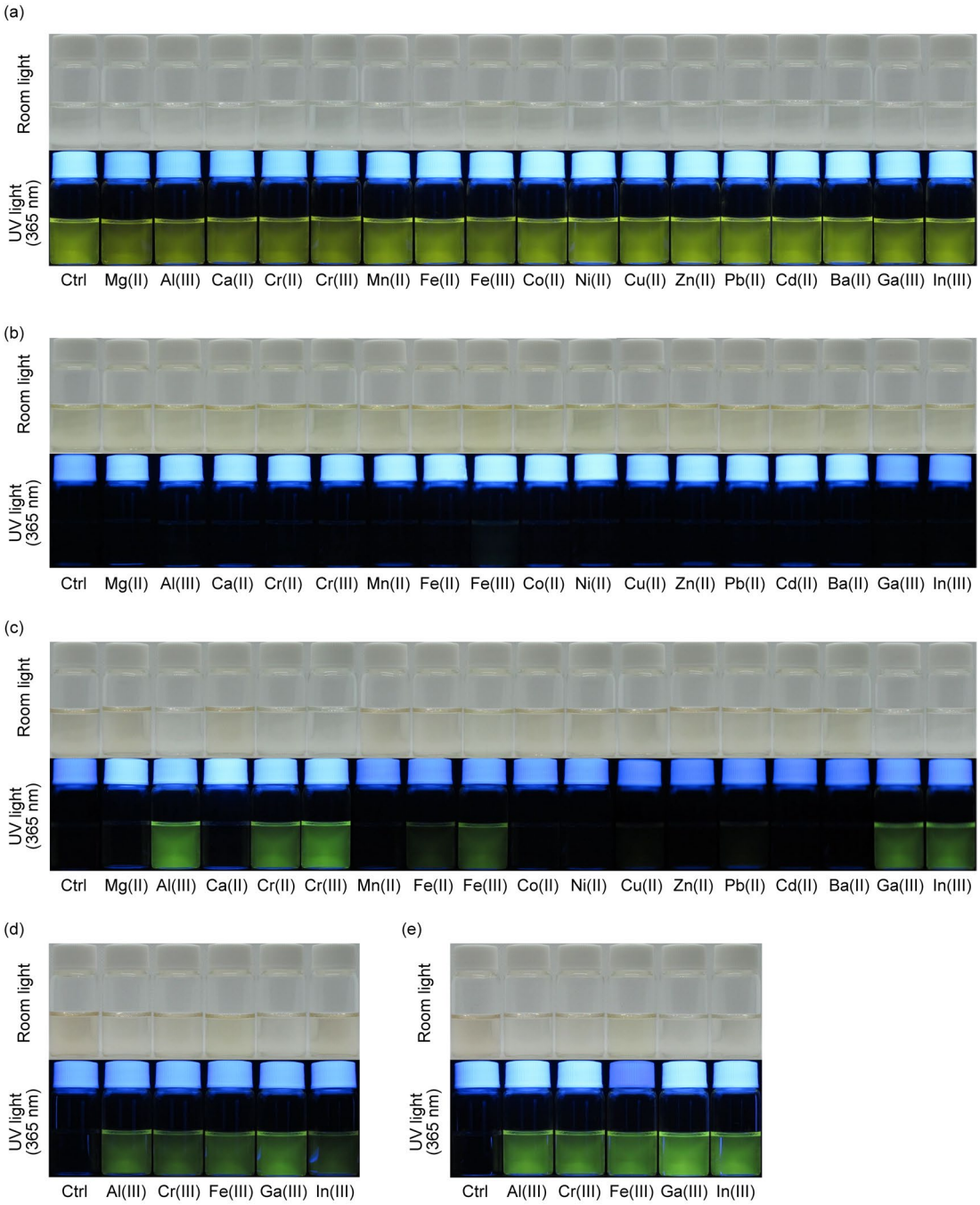

Figure S9. Pictures of **INA-Ph** (a), **-DMA** (b), **-DEA** (c), **-DPA** (d), and **-DBA** (e) solutions in vials under room light and UV light (365 nm) upon additions of the given di- and trivalent ions.

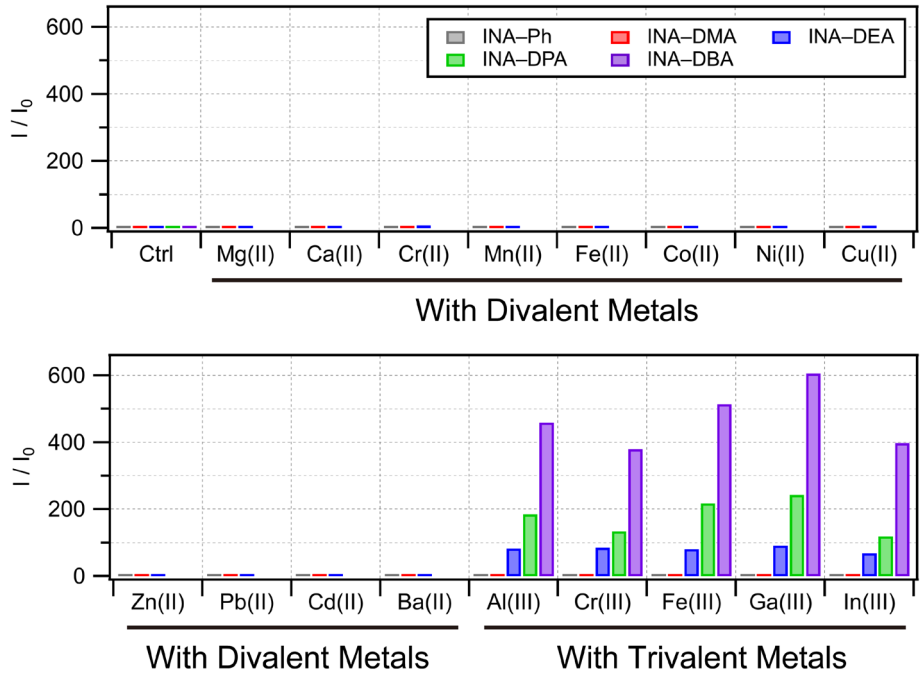

Figure S10. Fluorescence intensity (550 nm) of **INA** analogue solutions (20 μM) upon additions of di- and trivalent ions (5 equivalent).

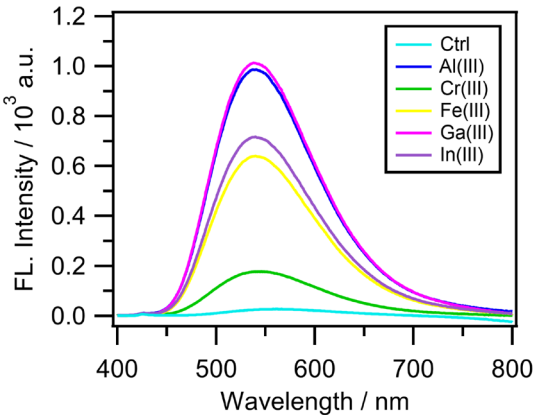

Figure S11. Fluorescence emission spectra of **INA-DEA** solutions (20 μM) upon addition of the given tri- and divalent metal ions (0.5 equivalents).

The competition assessments of the trivalent ions against the divalent ions

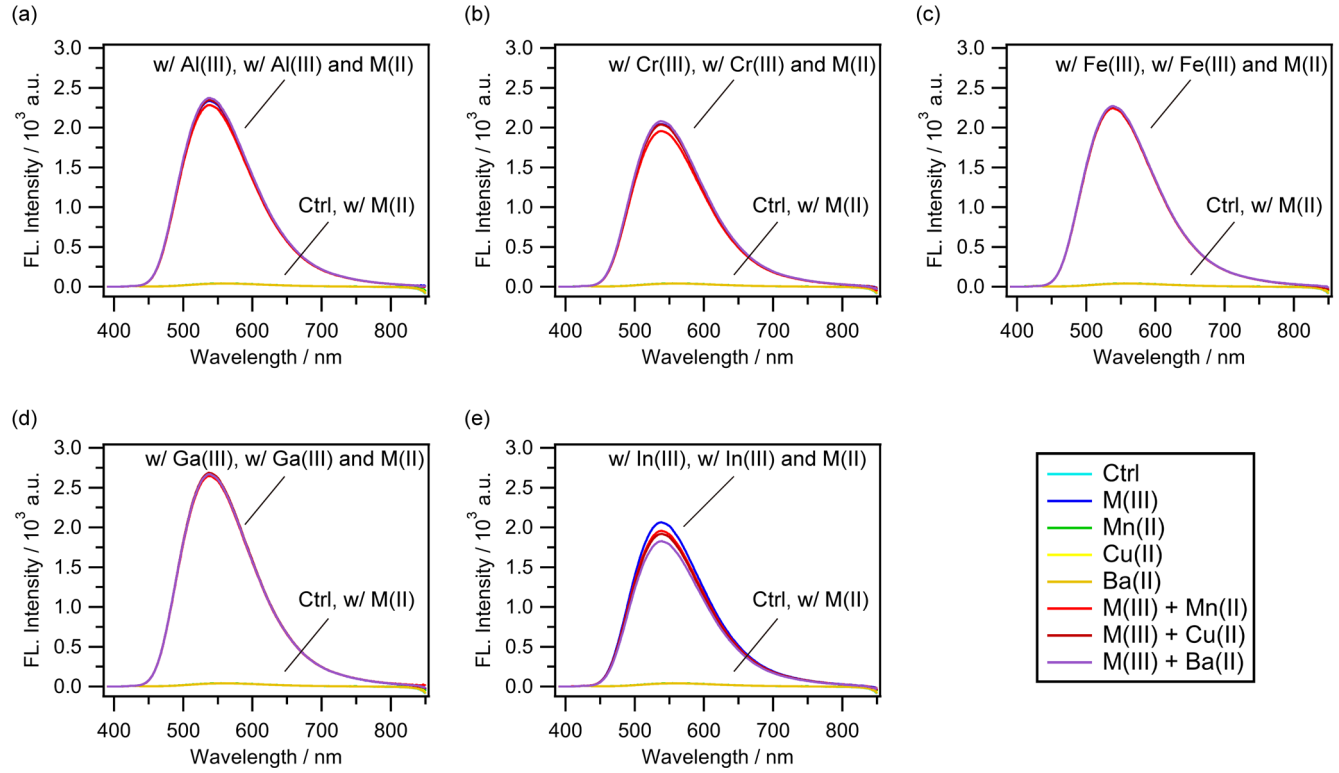

Figure S12. Fluorescence spectral changes of **INA-DEA** solutions (20 μM) with Al^{III} (100 μM) (a), Cr^{III} (100 μM) (b), Fe^{III} (100 μM) (c), Ga^{III} (100 μM) (d), and In^{III} (100 μM) (d) in the presence of different divalent ions (100 μM).

X-Ray Crystallography Data

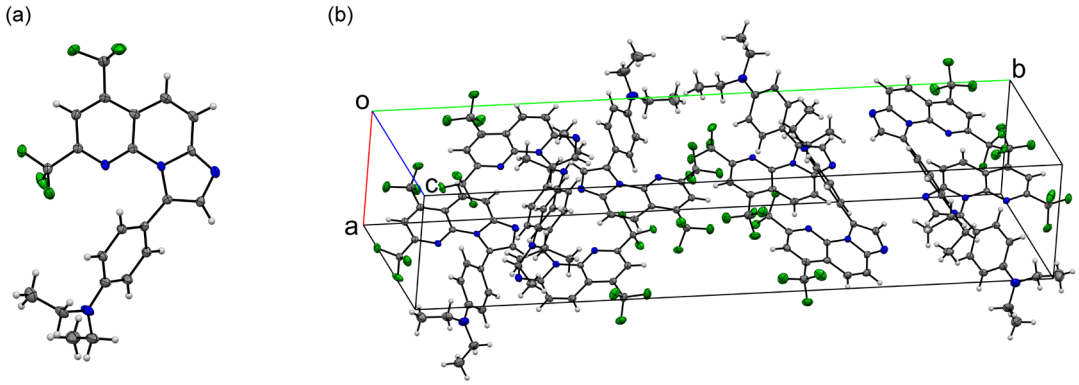

Figure S13. (a) ORTEP drawing (50% probability) of **INA-DEA** and (b) its molecular packings. The gray, blue, green, and white colors indicate C, N, F, and H atoms, respectively. Single red plate-shaped crystals of **INA-DEA** were obtained by recrystallisation from MeOH at rt. A suitable crystal 0.145×0.135×0.091 mm^3 was selected and mounted on a suitable support on an diffractometer.

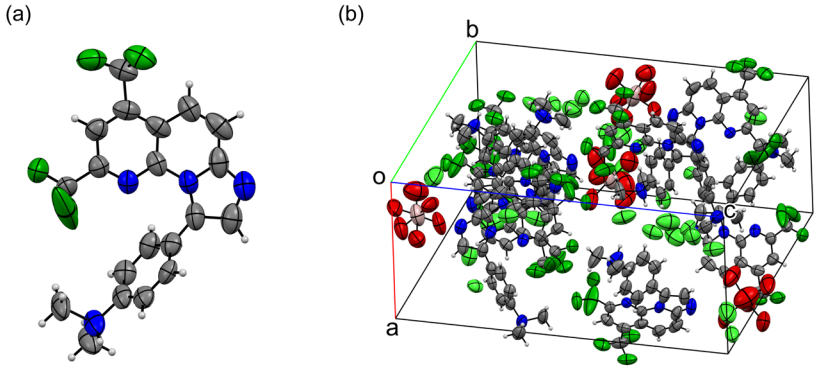

Figure S14. (a) ORTEP drawing (50% probability) of $[Al^{III}(H_2O)_6$ [**INA-DMA-H**]$^{+}{}_2]Cl_5$ and (b) its molecular packings. The gray, blue, green, red, pink and white coloured atoms indicate C, N, F, O, Al and H atoms, respectively. Single yellow block-shaped crystals of $[Al^{III}(H_2O)_6$ [**INA-DMA-H**]$^{+}{}_2]Cl_5$ were obtained by recrystallisation from MeOH solution of $AlCl_3$ at rt. A suitable crystal 0.165×0.063×0.051 mm^3 was selected and mounted on a suitable support on an diffractometer.

Table S6. Crystal data and structure refinement for **INA-DEA** and $[Al^{III}(H_2O)_6$ [**INA-DMA-H**$]^{+}{}_2]Cl_5$.

Compound	**INA-DEA**	$[Al^{III}(H_2O)_6$ [**INA-DMA-H**$]^{+}{}_2]Cl_5$
Empirical formula	$C_{22}H_{18}F_6N_4$	$C_{40}H_{30}N_8O_6F_{12}AlCl_5$
Formula weight	452.40	1150.95
Temperature/K	93	93(2)
Crystal system	monoclinic	orthorhombic
Space group	$P2_1$	$P2_12_12_1$
a/Å	7.65252(5)	10.67650(10)
b/Å	36.6358(2)	21.5837(3)
c/Å	14.87749(10)	24.0601(3)
α/°	90	90
β/°	104.4686(7)	90
γ/°	90	90
Volume/Å^3	4038.71(5)	5544.37(12)
Z	8	4
ρcalcg/cm^3	1.488	1.379
μ/mm^{-1}	1.123	3.335
F(000)	1856.0	2320.0
Crystal size/mm^3	0.145 × 0.135 × 0.091	0.165 × 0.063 × 0.051
Radiation/ Å	CuKα (λ = 1.54184)	CuKα (λ = 1.54184)
2Θ range for data collection/°	6.136 to 153.256	5.5 to 154.462
Index ranges	$-8 \le h \le 9$, $-43 \le k \le 44$, $-18 \le l \le 16$	$-13 \le h \le 11$, $-26 \le k \le 26$, $-29 \le l \le 29$
Reflections collected	22091	22241
Independent reflections	12134 [R_{int} = 0.0228, R_{sigma} = 0.0291]	10123 [R_{int} = 0.0215, R_{sigma} = 0.0283]
Data/restraints/parameters	12134/1/1162	10123/73/671
Goodness-of-fit on F^2	1.046	1.676
Final R indexes [I>=2σ (I)]	R_1 = 0.0311, wR_2 = 0.0838	R_1 = 0.1270, wR_2 = 0.3682
Final R indexes [all data]	R_1 = 0.0320, wR_2 = 0.0844	R_1 = 0.1387, wR_2 = 0.3879
Largest diff. peak/hole / e Å^{-3}	0.32/-0.22	0.85/-0.81
Flack parameter	-0.01(3)	0.105(10)

IR Spectra

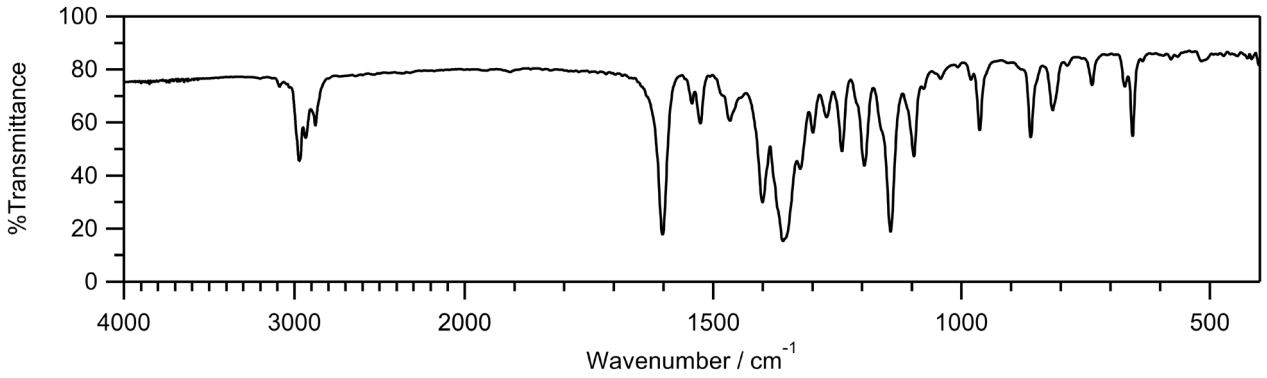

Figure S15. IR spectrum (KBr) of **1**.

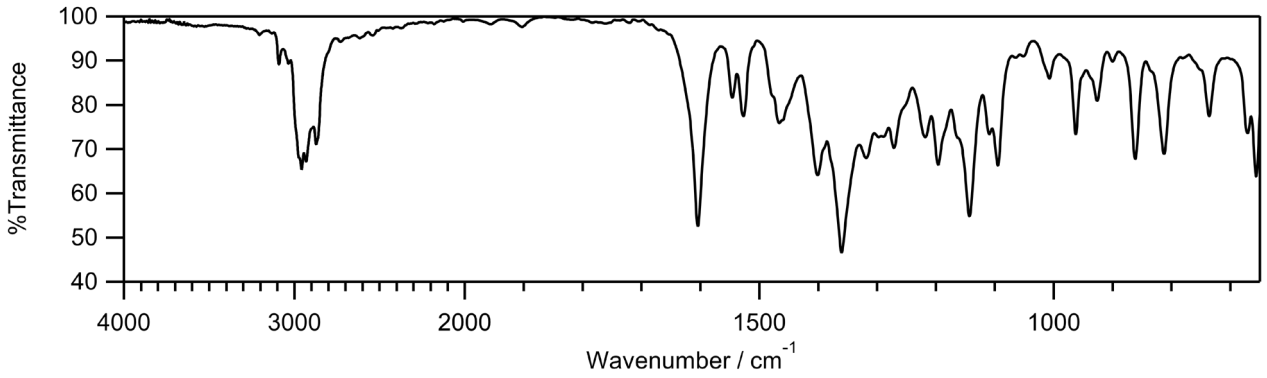

Figure S16. IR spectrum (NaCl) of **2**.

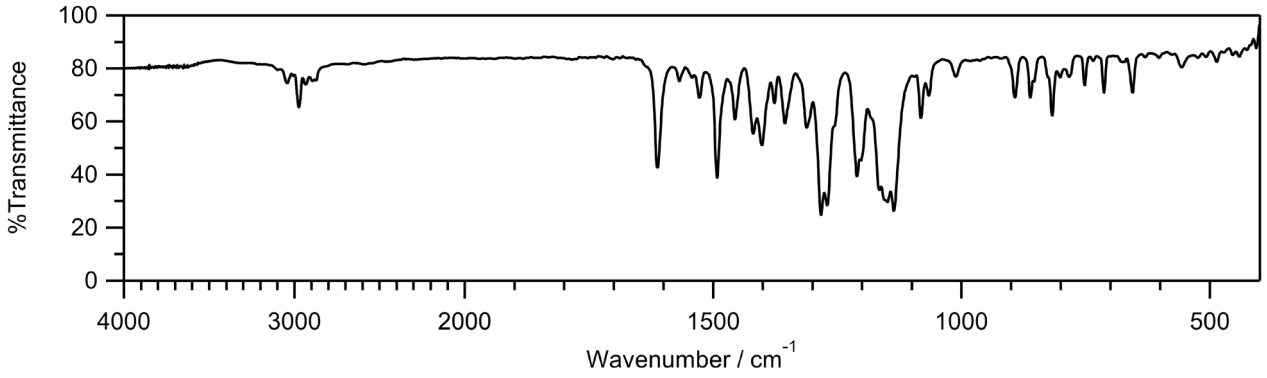

Figure S17. IR spectrum (KBr) of **INA-DEA**.

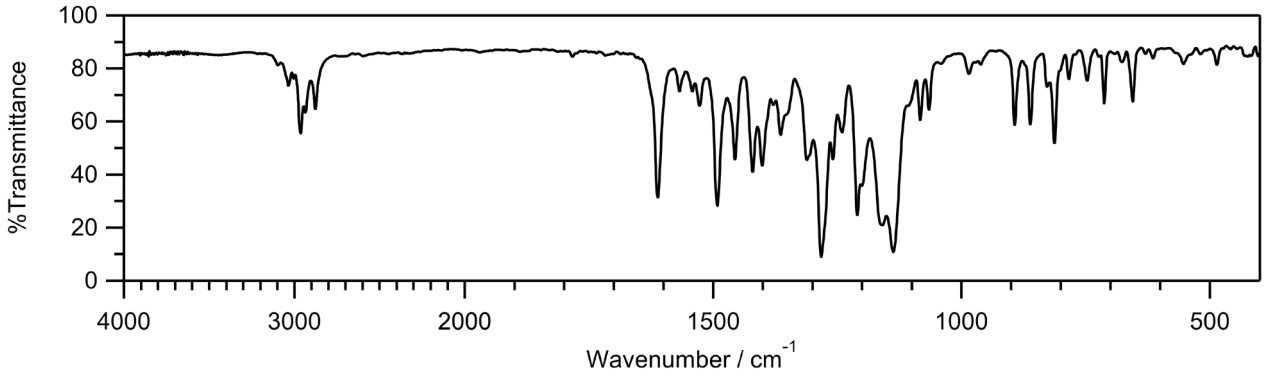

Figure S18. IR spectrum (KBr) of **INA-DPA**.

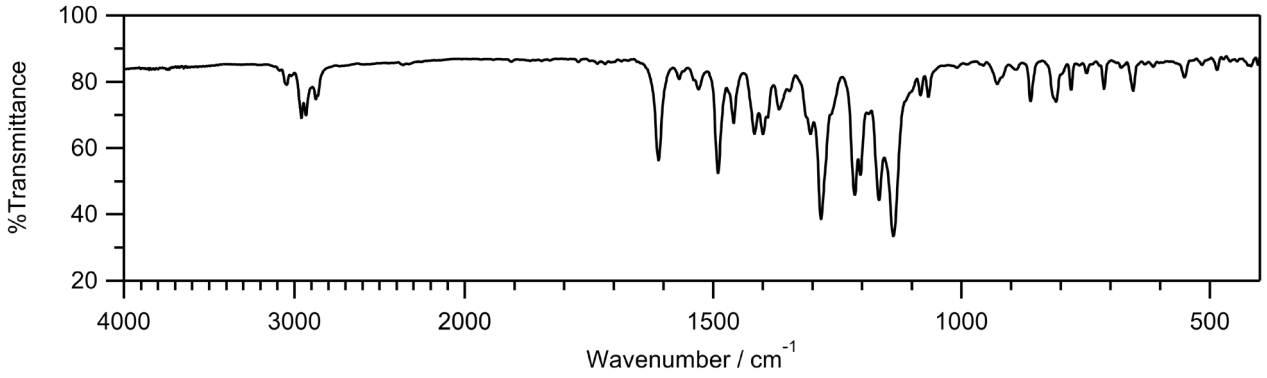

Figure S19. IR spectrum (KBr) of **INA-DBA**.

NMR Spectra

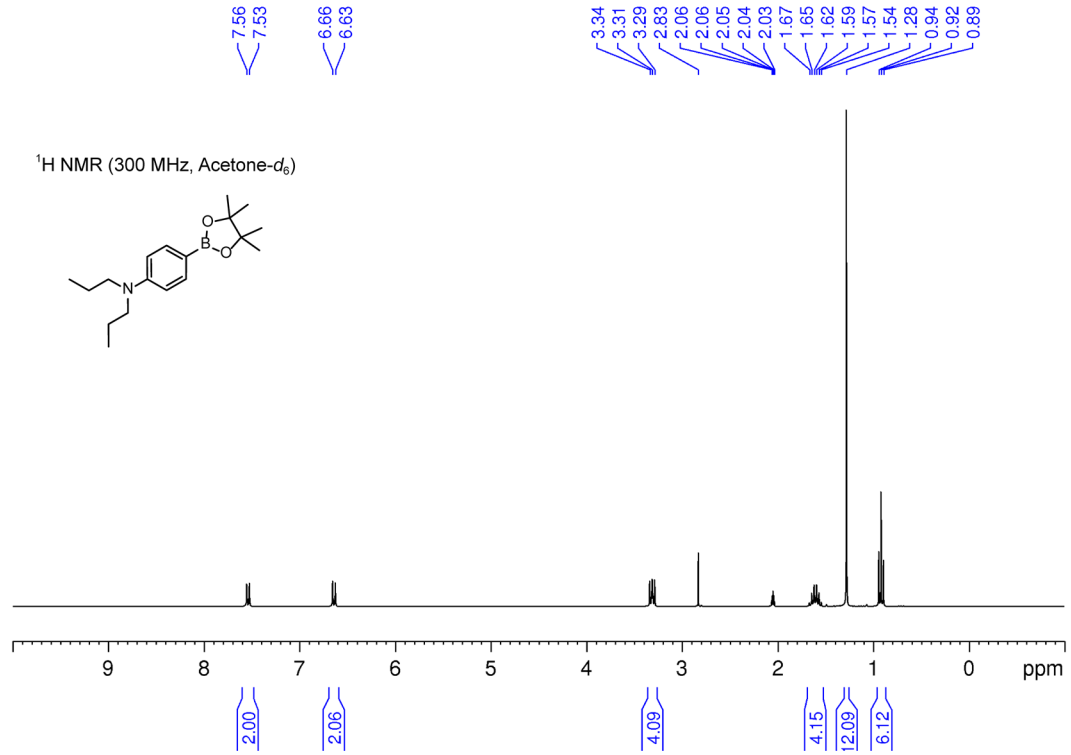

Figure S20. ^{1}H NMR spectrum (300 MHz) of **1** in Acetone-d_6.

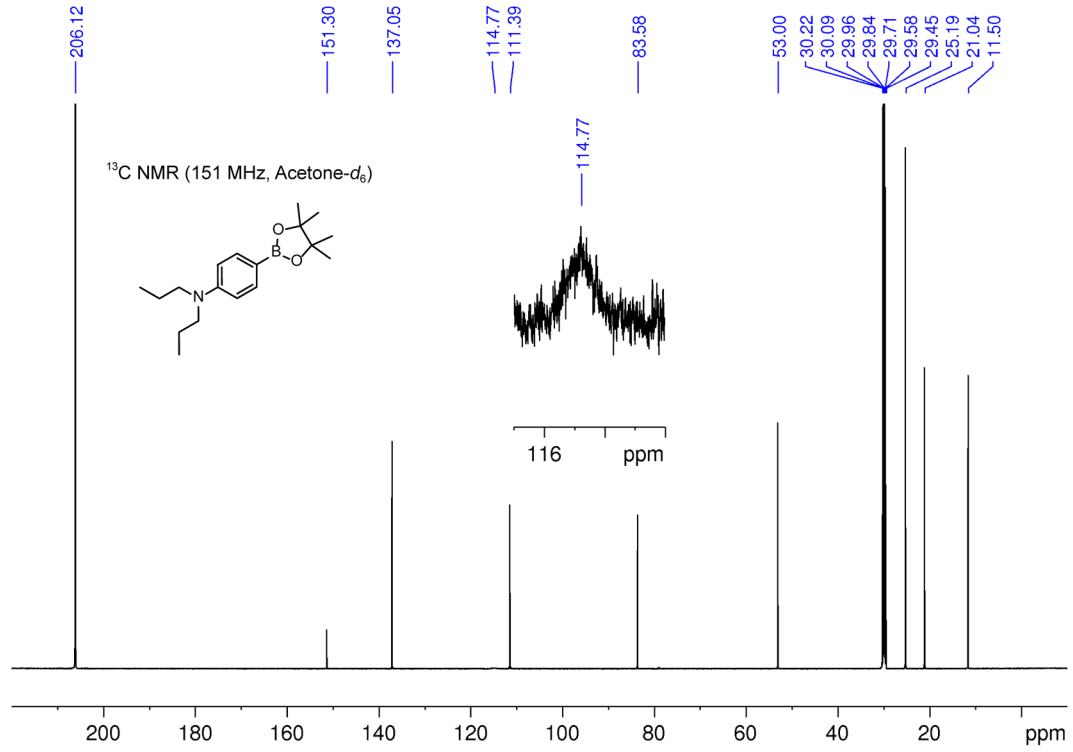

Figure S21. ^{13}C NMR spectrum (151 MHz) of **1** in Acetone-d_6.

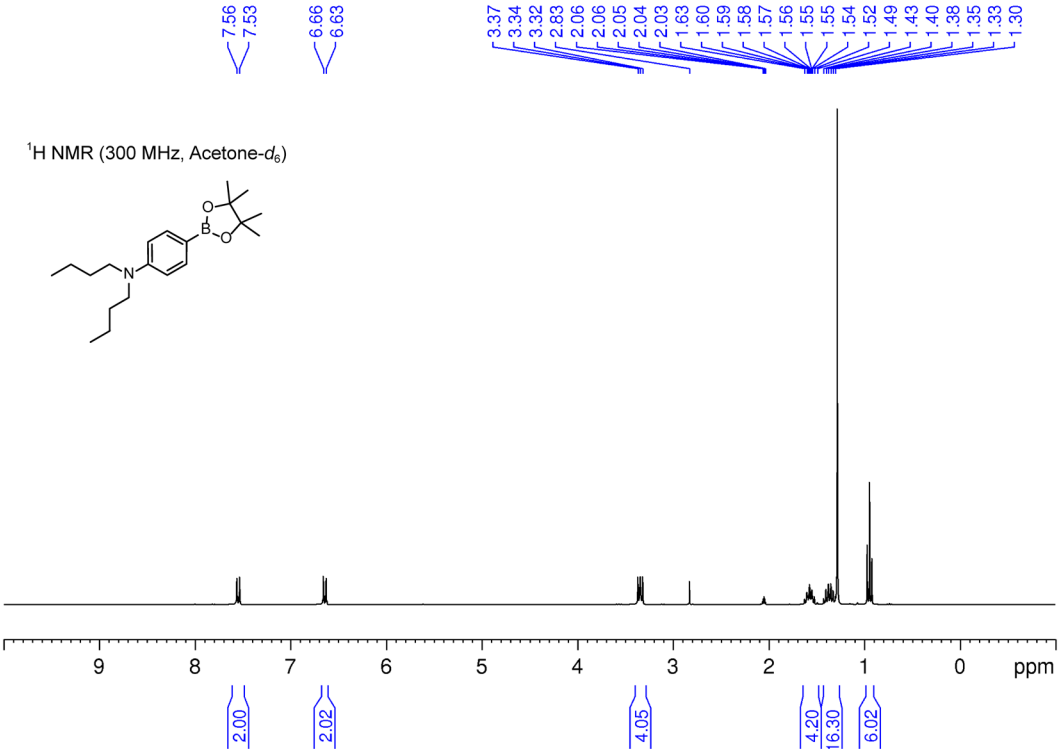

Figure S22. ^{1}H NMR spectrum (300 MHz) of **2** in Acetone-d_6.

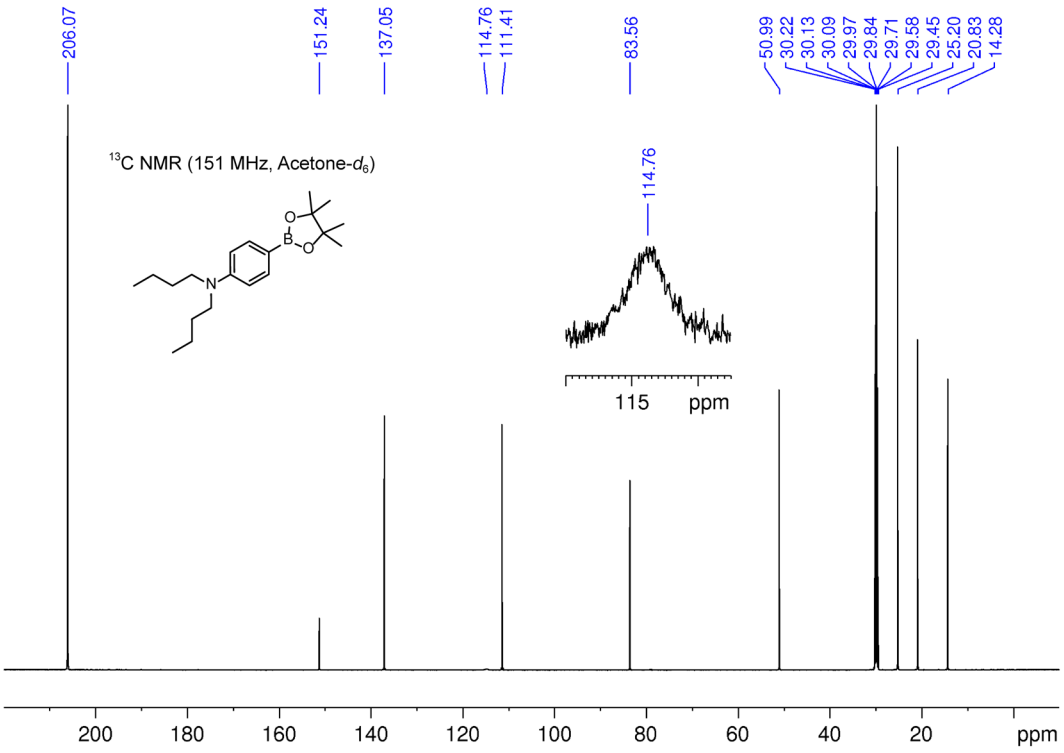

Figure S23. ^{13}C NMR spectrum (151 MHz) of **2** in Acetone-d_6.

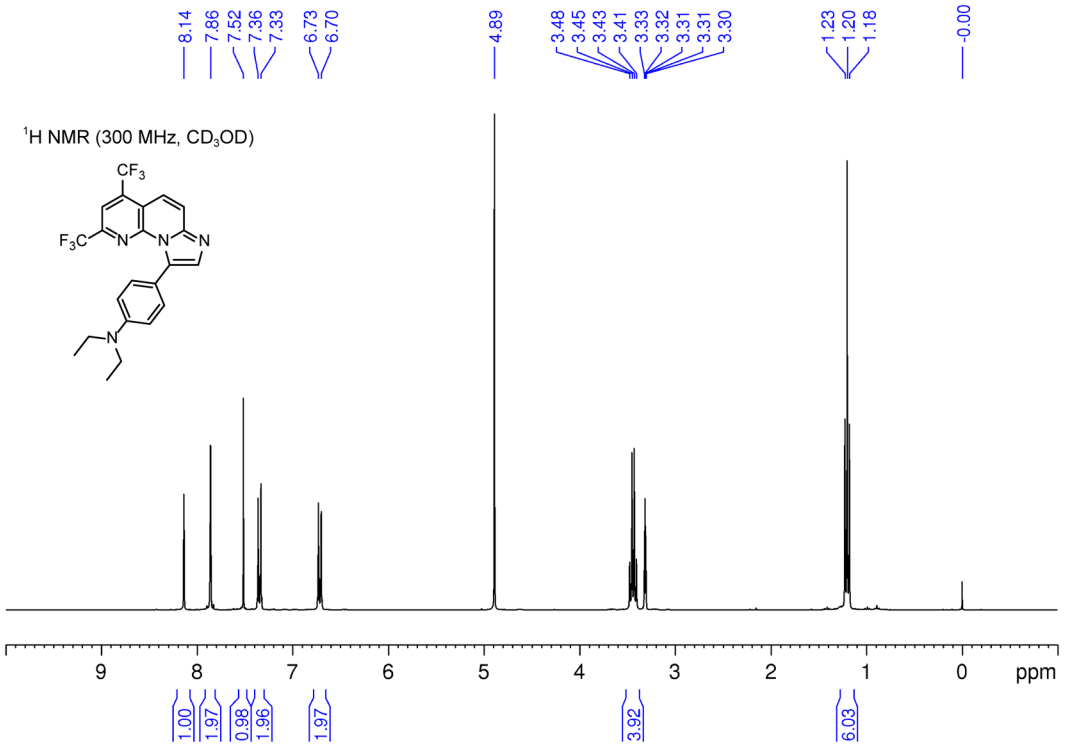

Figure S24. ^{1}H NMR spectrum (300 MHz) of **INA-DEA** in CD_3OD.

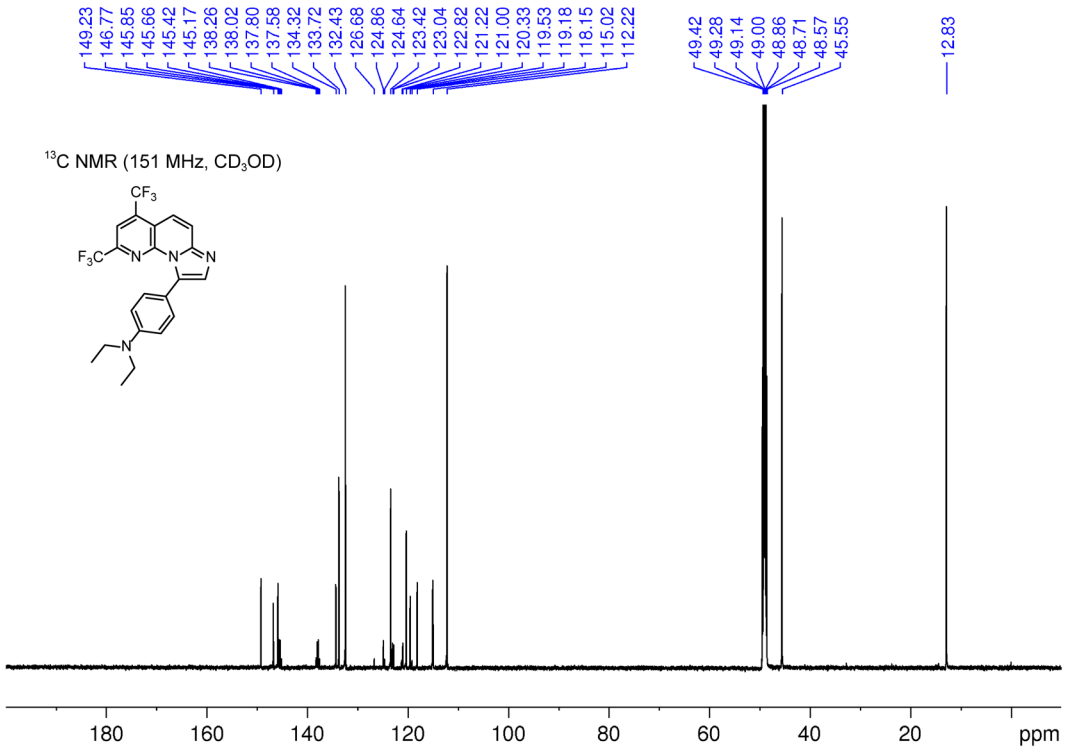

Figure S25. ^{13}C NMR spectrum (151 MHz) of **INA-DEA** in CD_3OD.

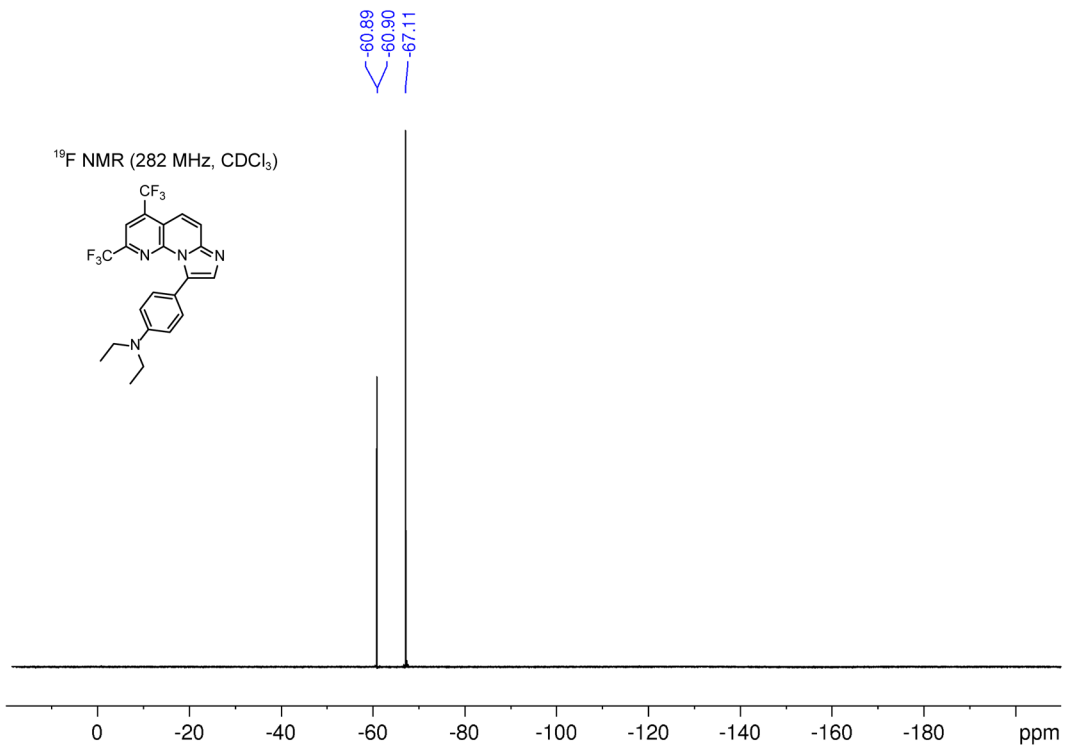

Figure S26. ^{19}F NMR spectrum (282 MHz) of **INA-DEA** in $CDCl_3$.

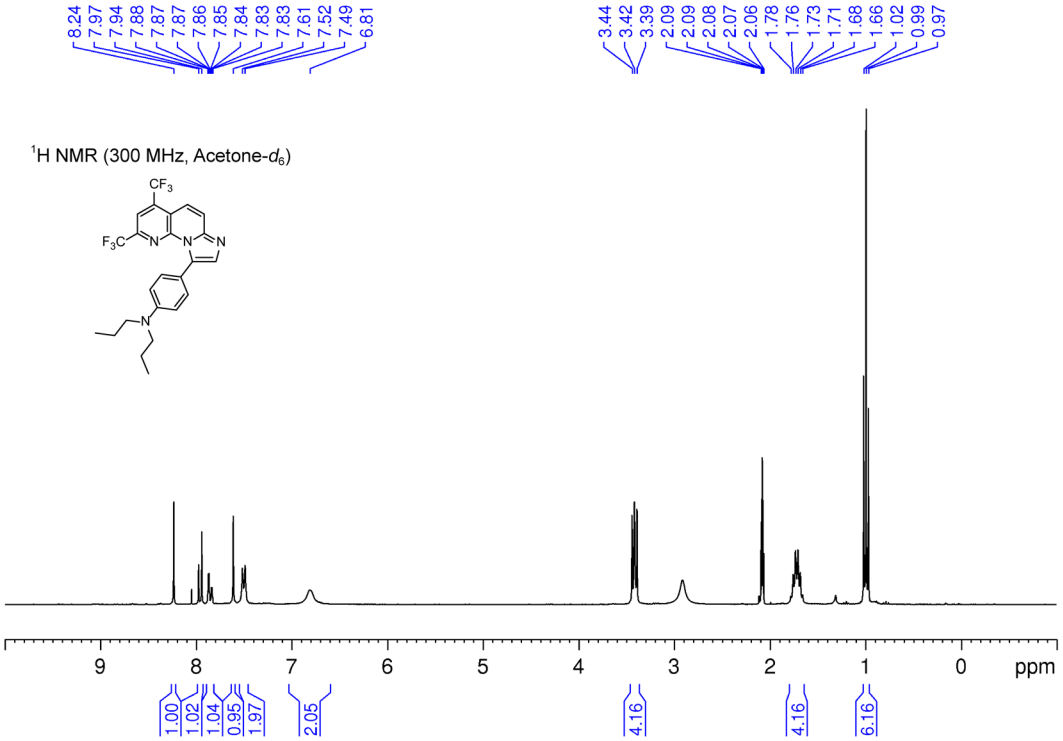

Figure S27. ^{1}H NMR spectrum (300 MHz) of **INA-DPA** in Acetone-d_6.

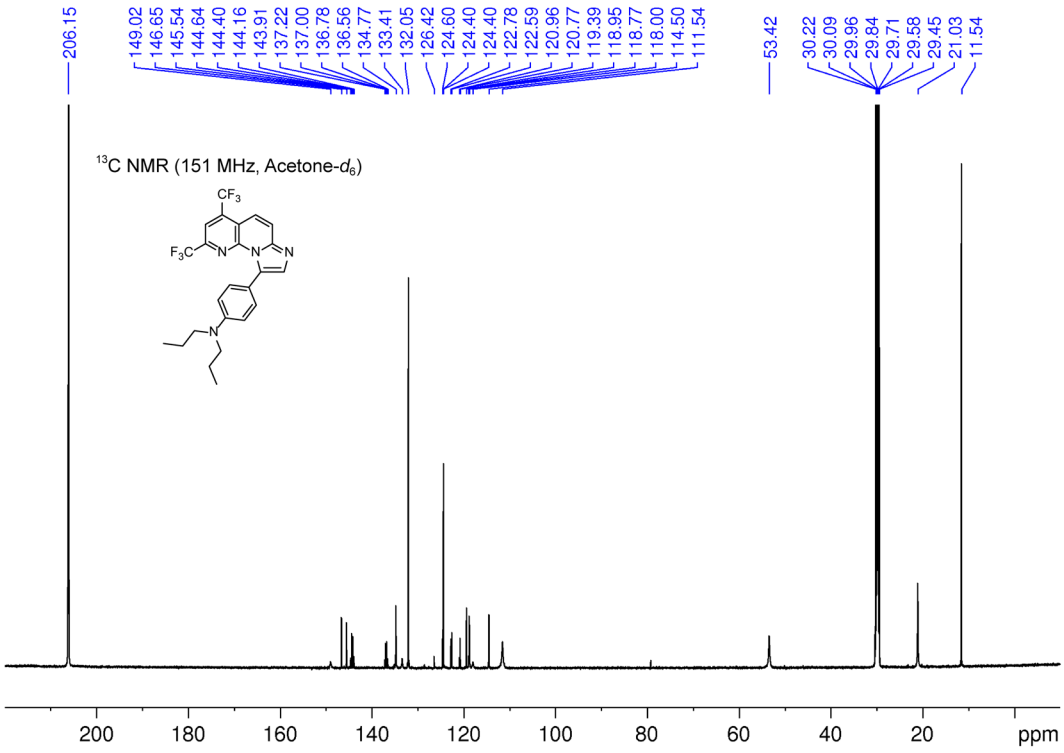

Figure S28. ^{13}C NMR spectrum (151 MHz) of **INA-DPA** in Acetone-d_6.

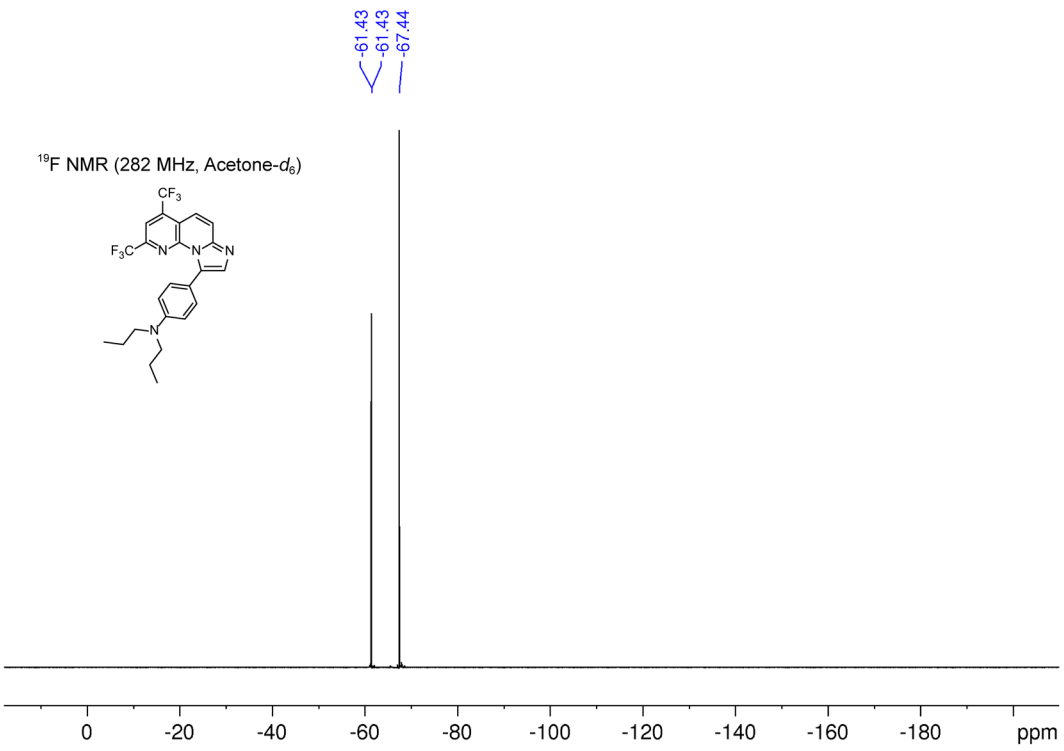

Figure S29. ^{19}F NMR spectrum (282 MHz) of **INA-DPA** in Acetone-d_6.

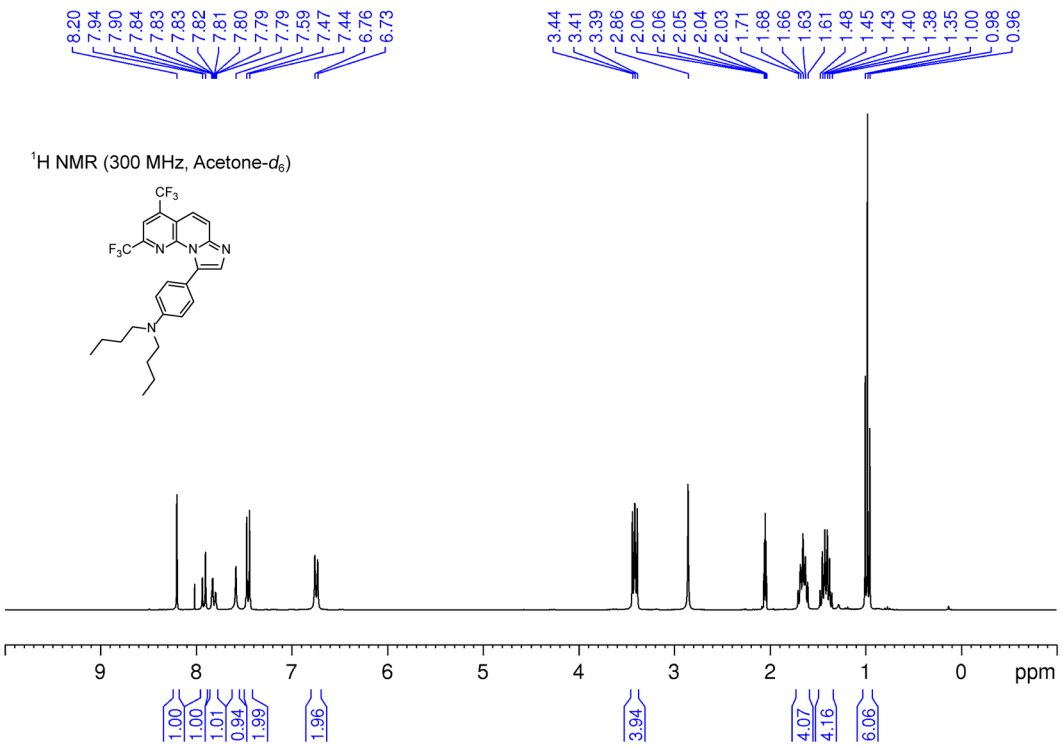

Figure S30. ^{1}H NMR spectrum (300 MHz) of **INA-DBA** in Acetone-d_6.

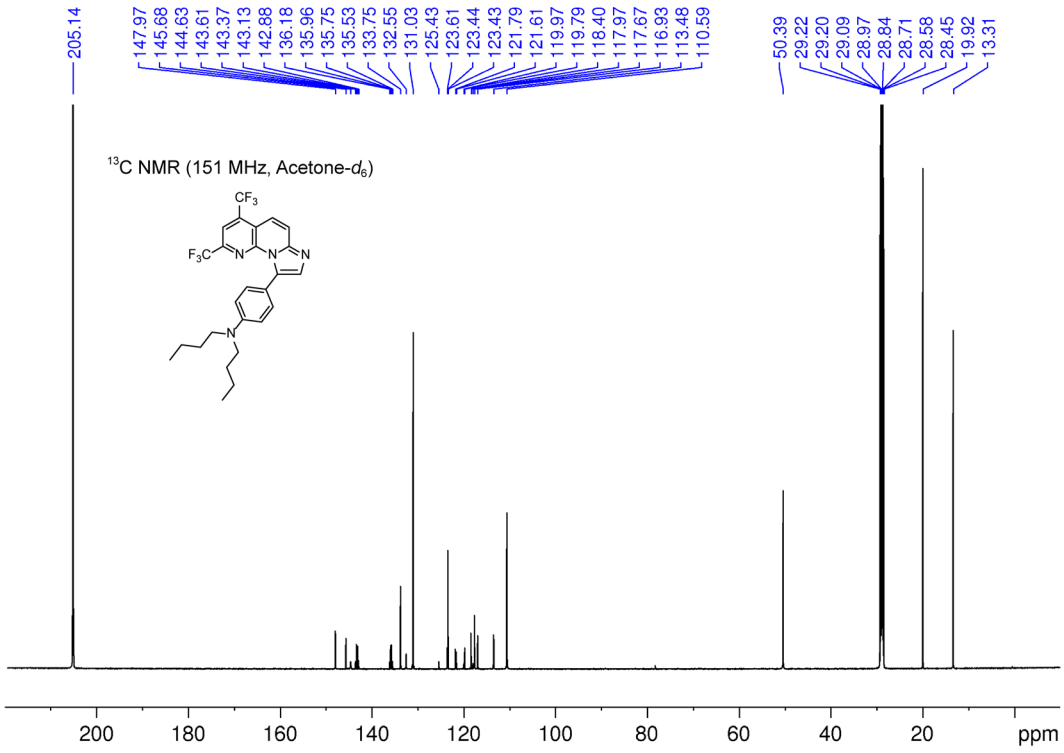

Figure S31. ^{13}C NMR spectrum (151 MHz) of **INA-DBA** in Acetone-d_6.

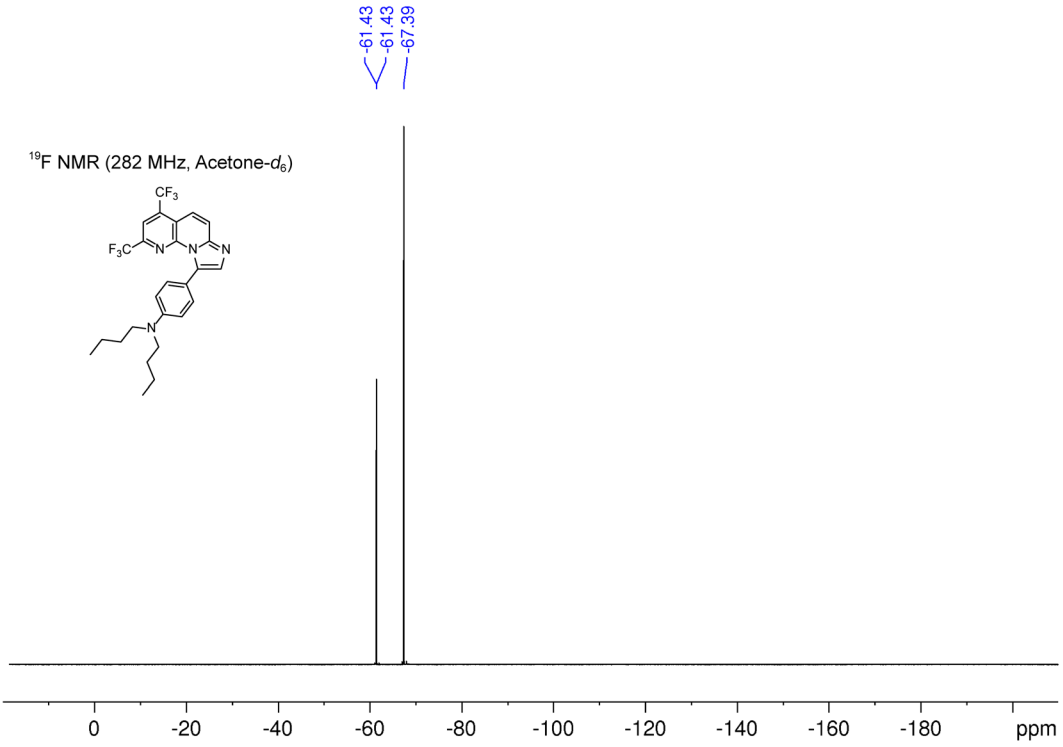

Figure S32. ^{19}F NMR spectrum (282 MHz) of **INA-DBA** in Acetone-d_6.

References

[1] G. M. Sheldrick, *Acta Crystallogr A Found Adv* **2015**, *71*, 3–8.
[2] O. V. Dolomanov, L. J. Bourhis, R. J. Gildea, J. A. K. Howard, H. Puschmann, *J. Appl. Crystallogr.* **2009**, *42*, 339–341.
[3] G. M. Sheldrick, *Acta Crystallogr. B* **2015**, *71*, 3–8.
[4] S. Matsumoto, T. Umeno, K. Usui, S. Karasawa, *Cryst. Growth Des.* **2021**, *21*, 5251–5260.
[5] J. W. Tomsho, A. Pal, D. G. Hall, S. J. Benkovic, *ACS Med. Chem. Lett.* **2012**, *3*, 48–52.
[6] N. Harada, Y. Abe, S. Karasawa, N. Koga, *Org. Lett.* **2012**, *14*, 6282–6285.
[7] S. Huang, J. Qing, S. Wang, H. Wang, L. Zhang, Y. Tang, *Org. Biomol. Chem.* **2014**, *12*, 2344–2348.